Analysis of the Sedimentary and Geochemical Characteristics of Sedimentary Clastic Rock Samples from the Alpha−Mendeleev Rise

M. I. Tuchkova[a, *], **S. G. Skolotnev**[a], **S. D. Sokolov**[a], **and S. A. Sergeev**[b]

[a] *Geological Institute, Russian Academy of Sciences, Moscow, 119017 Russia*
[b] *Karpinsky All-Russia Research Geological Institute, St. Petersburg, 199106 Russia*
***e-mail: tuchkova@ginras.ru**

Abstract—The paper presents new data on a comparative analysis of sedimentary rocks from the Mendeleev Rise (Shamshura Seamount), presumably, of the Triassic age with the Aptian sandstones obtained by the underwater sampling of the Alpha−Mendeleev Rise during expeditions in 2012, 2014, and 2016. The geochemical characteristics of rocks are very similar, and the data from different-age samples form common fields on various diagrams. Petrographic studies revealed that the sandstones of presumably Late Triassic age, as well as the sandstones of Chukotka and Wrangel Island, are dominated by fragments of shale and felsic effusives. The Aptian samples are dominated by mafic rock fragments. In addition, sharp differences are observed in the age spectra of detrital zircon populations, indicating fundamentally different provenances for the Triassic and Cretaceous sandstones on the Alpha−Mendeleev Rise. Samples from the Shamshura Seamount are characterized by populations similar to those from Triassic rocks of Chukotka and Wrangel Island, suggesting the presence of Triassic rocks in this part of the Mendeleev Rise.

INTRODUCTION

The underwater sampling of the Alpha−Mendeleev Rise was carried out in 2012, 2014, and 2016, using manipulators of a research submarine and sampling from an icebreaker using the grab sampler, dredger, and drilling device (Morozov et al., 2013; Skolotnev et al., 2017). The sample collection obtained during these expeditions revealed the presence of sedimentary and igneous rocks. Sedimentary rocks are represented by dolomites, limestones, quartzite-type sandstones, and sandstones. Faunal remains were found in some carbonate rock samples, making it possible to determine the age of host rocks. According to different authors, sedimentary rocks were formed at the Upper Silurian−Permian stratigraphic interval (Kossovaya et al., 2018) or at the Upper Ordovician−Lower Cretaceous interval with several hiatuses (Skolotnev et al., 2019, 2022).

Detrital zircon grains were separated from some clastic rock samples from the 2012 collection and their U/Pb isotopic age was determined with the SHRIMP mass spectrometer at the Isotope Analytical Center, Karpinsky All-Russia Research Geological Institute, St. Petersburg. Based on the data stored at this insti-

tute, the fine-grained sandstones (samples USO-4, SS-63, and SS-65) taken from the Shamshura Seamount (Fig. 1) contain numerous (and youngest) zircon population with the age range of 206−246 Ma. By analogy with the regional data, the above fact suggests that such zircons can be assigned to the Late Triassic stratigraphic interval. The detailed petrographic and geochemical analysis of these samples revealed their great similarity to the coeval sandstones of Wrangel Island and Chukotka (Tuchkova et al., 2020). Moreover, researchers could trace the regular shallowing of the Late Triassic sedimentary basin from the south to north, and assume the proximity of the continental land to the northeast of the Mendeleev Rise.

During expeditions in 2014 and 2016, S.G. Skolotnev recovered Paleozoic and Cretaceous rock samples at three different polygons of the Alpha−Mendeleev Rise using the research submarine (Skolotnev et al., 2022). During 2014 and 2016, Cretaceous sandstones were recovered from the southwestern (samples 14-09 and 14-24, polygon 1) and central (samples 1601/1 and 1601/10, polygon 3) parts of the Mendeleev Rise, as well as from the Trukshin Seamount (sample 1602/14, polygon 2) in the polar part of the Alpha Ridge (Skolotnev et al., 2017, 2022). Sample 1602/14
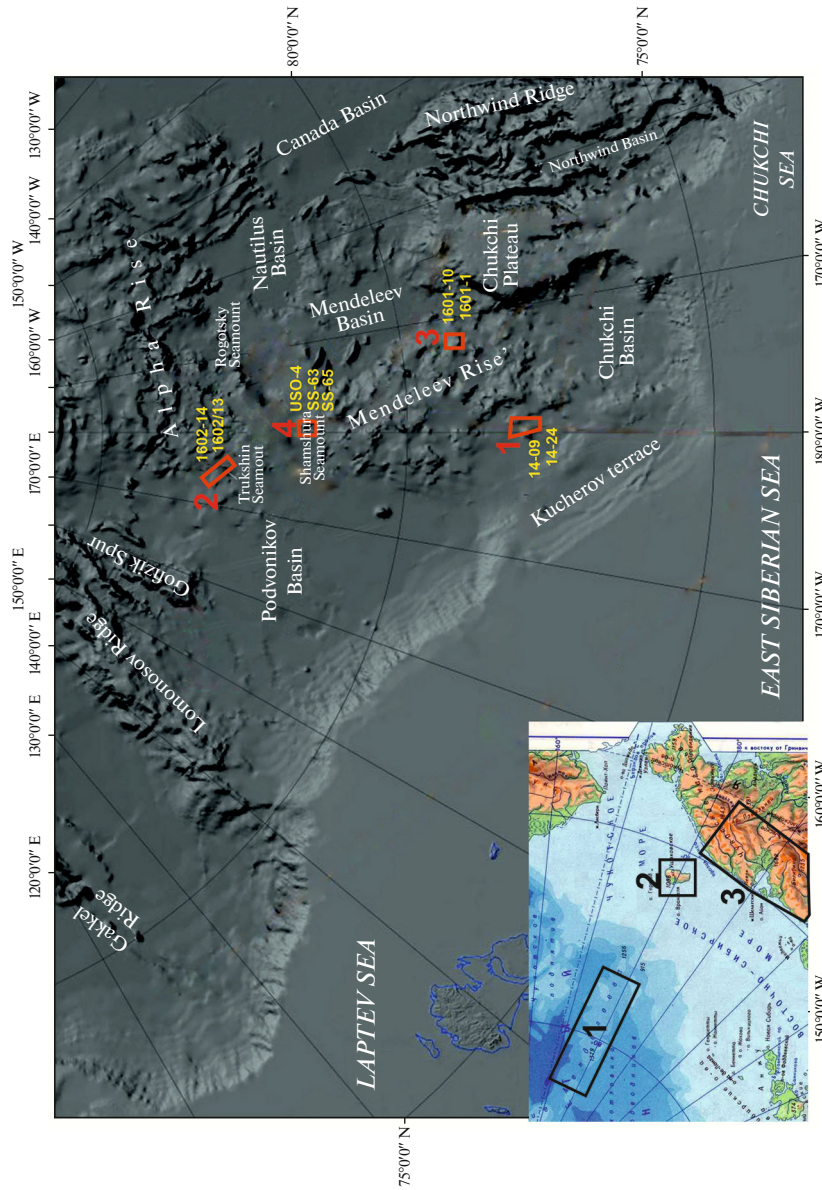
Fig. 1. Positions of the analyzed samples on the geographic map of uplifts in the Central Arctic, based on the IBCAO survey map http://www.ngdc.noaa.gov/mgg/bathymetry/arkosic/. Positions of detailed work sites on the Alpha–Mendeleev Rise are shown by red boxes—Fig. 1 is adopted from (Skolotnev et al., 2022). Samples numbers (shown in yellow) correspond to those in the section (Skolotnev et al., 2022). The inset shows a fragment of the geographic map of the Russian Arctic region with samples used in this article: (1) Alpha–Mendeleev Rise, (2) Wrangel Island, (3) Chukotka.

Table 1. Mineral composition of sandstones on the Alpha−Mendeleev Rise

Major components	Sample no.				
	USO-4	SS-65	1602-14	1601-10	14-09
Quartz	56 (55.8%)	52 (41.3%)	148 (53.6%)	186 (79.8%)	92 (39.5%)
Feldspars	14 (10.9%)	35 (27.8%)	68 (24.6%)	22 (9.44%)	11 (4.7%)
Micaceous and chlorite schists	20	6	2		21
Clasts with chlorite in the matrix					0
Felsic effusives	11	2	5		10
Mafic effusives	8		29	2	58
Granitoids	11	20	15	1	24
Cherts	3		2		3
Mica	5 (3.9%)	1 (0.8%)	7 (2.5%)	5 (2.14%)	12 (5%)
Accessory minerals	3		4		
Fragments of silty mudstone (synsedimentary)		10		17	2
Total rock fragments	58 (45.3%)	39 (30.9%)	60 (21.7%)	25 (10.7%)	130 (55.8%)
Total calculated grains	131	126	280	233	233

contains the Barremian−Aptian palynomorphs (Sko-lotnev et al., 2019). For samples 14-24 and 1602/14, the Cretaceous age was determined based on the U−Pb dating at the above Isotope Analytical Center (St. Petersburg), since they contain a young zircon population of the 100−126 Ma age range. The age of the young zircon population coincides with the age based on the palynomorphs. For the remaining four samples (14-09, 1601/1, 1601/10, and 1602/13), their belonging to the Cretaceous stratigraphic interval is established based on their spatial and petrographic closeness to Cretaceous sandstones.

Since the petrographic characteristics of Creta-ceous sandstones and sandy limestones are very simi-lar to sandstones on the Shamshura Seamount, the Late Triassic age of samples (USO-4, SS-63, and SS-65) dated earlier (Tuchkova et al., 2020) became doubtful. Moreover, Aptian sandstones are exposed with a spacing of 5−20 m slightly above the Paleozoic rocks, leaving virtually no space for the location of rocks of the intermediate age. Therefore, during addi-tional studies aimed at scrutinization of the composi-tion and age of Mesozoic sandstones on the Alpha−Mendeleev Rise (the results are presented in this arti-cle), we attempted to confirm or refute the Triassic age of samples from the Shamshura Seamount.

PETROGRAPHIC CHARACTERISTICS OF ROCKS

All analyzed sandstones have the fine-grained tex-ture with the carbonate cement. The mineral compo-sition is dominated by quartz grains, some of which are angular (Fig. 2).

Triassic fine-grained sandstones of the Shamshura Seamount are characterized by the quartz−feldspar composition (samples USO-4, SS-63, and SS-65, Table 1) and the carbonate basal cement of the calcite

or dolomite composition in some places. The rock-forming components have the following composition: quartz (41−56%), feldspar (11−28%), rock fragments (31−45%), crystalline schists, granites, felsic and mafic effusives, and mica (1−4%). The volcanic glass is chloritized in fragments of the mafic effusives. The clastic quartz grains are crosscut by microfractures (15−31%) filled with a mixture of clay minerals. The feldspars therein can be replaced by kaolinite along the periphery and in the central part of the grain (Tuch-kova et al., 2020).

Cretaceous sandstones are characterized by the quartz or quartz−feldspar composition (Table 1). They are represented by calcareous sandstones (sam-ples 14-24, 1602/13, and 1602/14), clayey sandstones (1601/1 and 1601/10), as well as intermediate-type (calcareous−clayey) sandstones (sample 14-09) (Sko-lotnev et al., 2022). The studied thin sections show the basal carbonate cement (up to 20−40 vol % in samples 14-24 and 1602/14). In samples 1601/10 and 14-09, the amount of cement is significantly less (not more than 15−20 vol %). In sample 1602/13, the carbonate dominates (as much as ~90 vol % in some sections), although, in general, the terrigenous/carbonate com-ponent ratio in the sample is approximately the same (Skolotnev et al., 2022). In thin sections, one can see microbedding and even graded bedding in some places (sample 1601/10), with lenses and laminas of silty clays. Fragments of silty clays are represented by irreg-ular smectite−chlorite aggregates, which fill up the gaps between grains, creating the effect of cement. Such fragments also contain a small amount of clastic grains up 0.05 mm in size.

The sandstones are dominated by quartz, often angular (Figs. 2a, 2b), with the grain size of 0.05−0.15 mm. The larger (0.2−0.22 mm) subrounded grains with overgrowths are rare. Quartz grains with microfractures, characteristic of sandstones on the
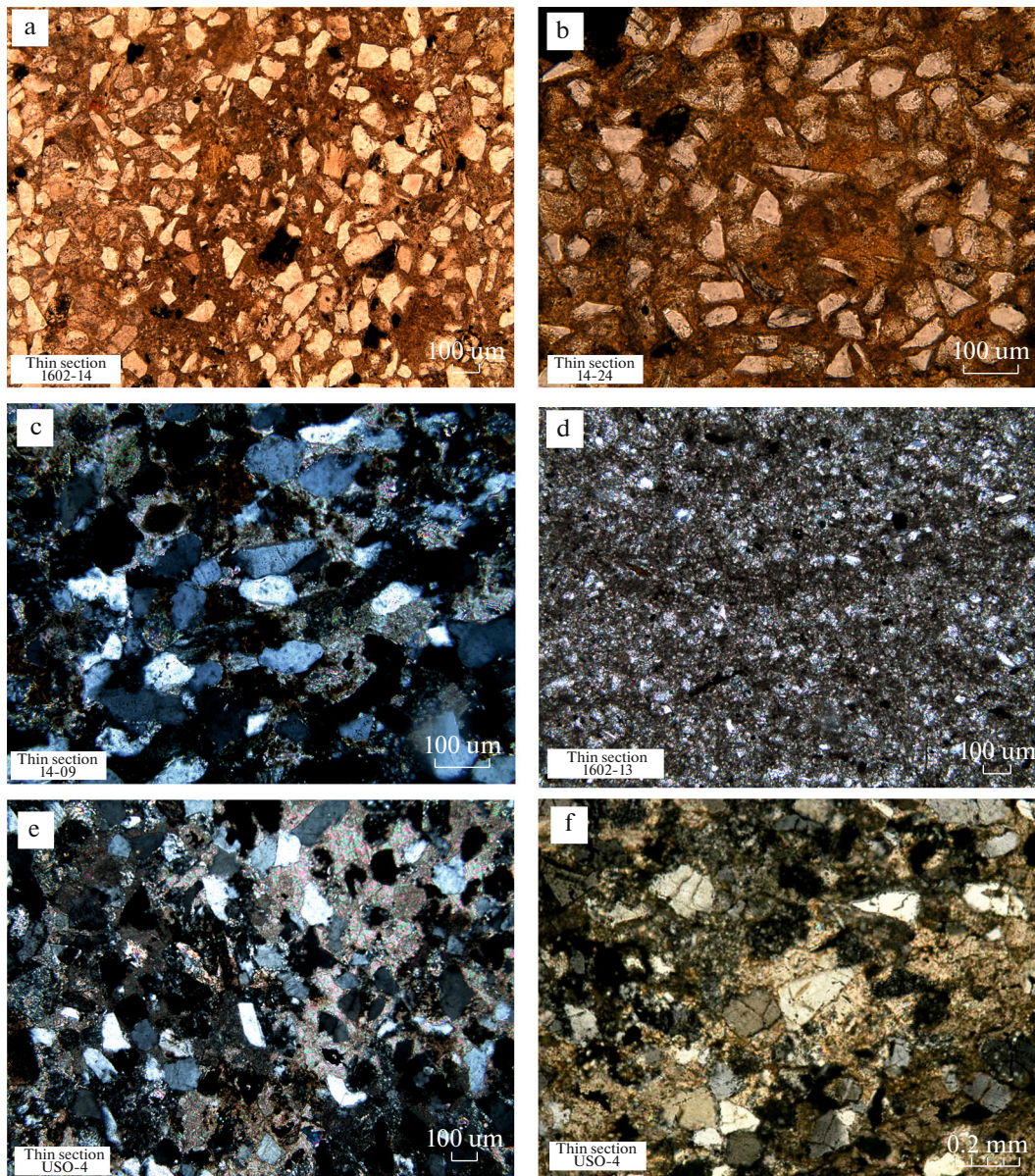
Fig. 2. Photomicrographs of sandstones from the Alpha−Mendeleev Rise. (a) Well-sorted quartz−feldspar sandstone with the smectite−chlorite basal cement replaced by calcite, numerous angular quartz grains with sharp edges, sample 1602/14, plane-polarized light; (b) fine-grained quartz−feldspar silty sandstone cemented with the smectite−chlorite mass replaced by calcite, quartz grains are predominantly angular, sample 14-24, plane-polarized light; (c) fine-grained quartz−feldspar sandstone cemented with aggregates of iron hydroxides and ferruginous carbonate, quartz grains are predominantly rounded and angular with smooth edges, corroded with ferruginous carbonate, sample 14-09, crossed polars; (d) micritic limestone with the terrigenous admixture (10−15%), microbedding and traces of bioturbation, sample 1602/13, plane polarized light; (e) quartz−feldspathic silty sandstone with the basal calcite and dolomite cement, corroded in some places; quartz grains are rounded, rarely angular and corroded, quartz grains with microfractures are rare, sample USO-4, crossed polars; (f) quartz−feldspar silty sandstone with angular quartz grains and microfractures, sample USO-4, crossed polars.

Shamshura Seamount (USO-4 and SS-65), are almost absent in samples of the Cretaceous age, although some such grains were noted in sample 1601/10. In addition to quartz, the sandstones contain the intermediate plagioclases, microcline, and microcline−plagioclase intergrowths. The rocks also contain the dehydrated biotite (samples 1601/10 and 1602/14), or biotite and muscovite (sample 14-24), pyroxene grains (sample 1601/10), feldspar−pyroxene aggregates, fragments of volcanic glass replaced by chlorite, and microlithic fragments (sample 1602/14). Sample 14-09 is marked by a high content of rock fragments that are replaced commonly by chlorite, hampering their identification. However, relicts of the pri-
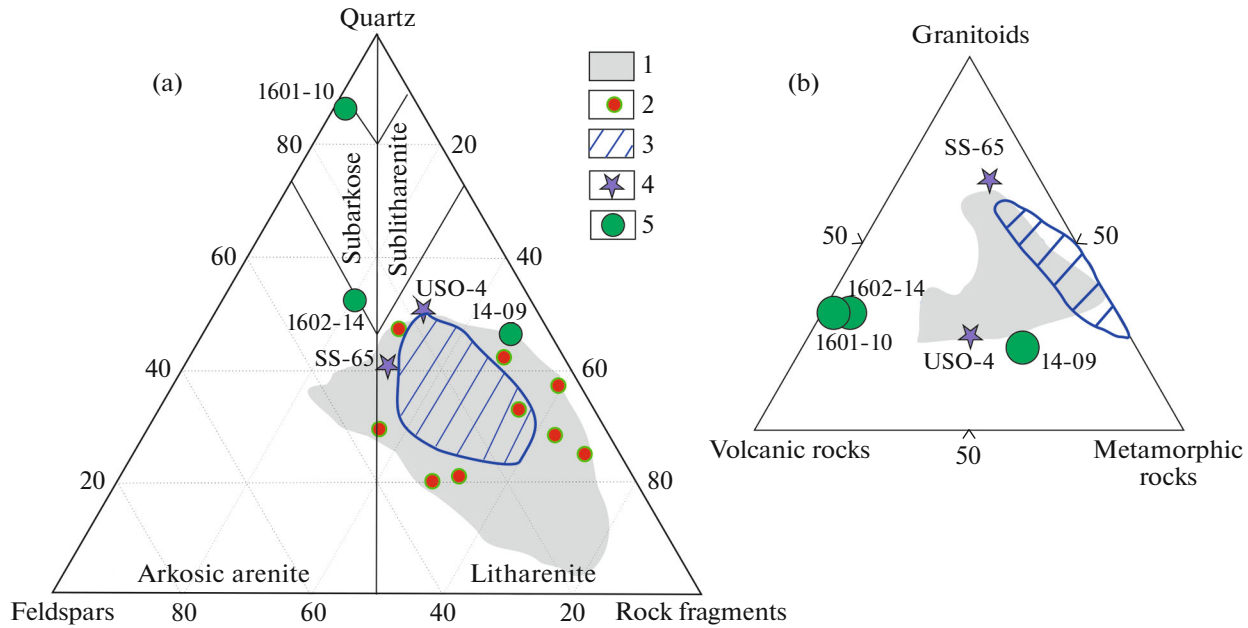
Fig. 3. Composition diagrams of sandstones. (a) Diagram of sandstone classification: (quartz−feldspars−rock fragments), rock fields are drawn according to the classification diagram (Pettijohn, 1975); (b) the ratio of rock fragments in sandstones. (1) Composition field of Upper Triassic sandstones in Chukotka, according to (Tuchkova et al., 2023); (2) Lower−Middle Triassic sandstones in Chukotka, according to (Tuchkova et al., 2023); (3) composition field of Upper Cassis sandstones in Wrangel Island, according to (Tuchkova et al., 2023); (4) composition of conditionally Triassic sandstones from the Alpha−Mendeleev Rise (Shamshura Seamount); (5) composition of Cretaceous sandstones from the Alpha−Mendeleev Rise.

mary texture make it possible to classify them as volcanic rocks (Table 1), although it is difficult to determine their type because of their small size. The thin sections show a high content of heavy minerals and isotropic iron hydroxide aggregates of various shapes, probably, replacing the weakly lithified clay fragments (about 0.1 mm in size) formed together with the sediment, as evidenced by their structural position in the rock. One can also see quite large (rounded or irregular) aggregates (0.3−1 mm) of organic matter randomly distributed in the rock.

Sample 1602/13 (polygon 2) is represented by the calcareous sandstone with traces of bioturbation (Fig. 2d) and a terrigenous impurity (10−15%). The grain size is 0.03−0.05 mm. The thin section shows a thin microbedding with alternating darker and lighter bands. Angular fragments of quartz, tabular intermediate plagioclases, muscovite-type micas, and iron hydroxide aggregates are confined to the light bands. The dark bands are characterized by an increased content of organic matter of different sizes and shapes, as well as small carbonate lumps (0.01−0.03 mm).

On the classification diagram of the rock-forming components (Fig. 3a) drawn according to (Pettijohn, 1975), the analyzed samples fall into the fields of subarkosic sandstones (sample 1601/10), as well as arkosic arenites (sample 1602/14) and litharenites (samples 14-09, USO-4, and SS-65).

In the diagram, with the vertices marked by fragments of effusives, metamorphic rocks, and granitoids, the analyzed samples form different groups (Fig. 3b): one group is characterized by the minimum content of volcanic fragments; another group, by their high content. The first group includes Triassic rock samples from Chukotka and Wrangel Island. Sample USO-4 belongs to this group, but a sample SS-65, characterized by a high content of granitoid fragments, occupies a separate position. Samples of the second group with a high content of volcanic fragments make up a separate cluster of Cretaceous sandstones from the Alpha−Mendeleev Rise.

GEOCHEMICAL CHARACTERISTICS OF ROCKS

Concentrations of the rare earth elements (REE) in the Cretaceous sandstones were determined by the ICP-MS method using the Element2 mass spectrometer at the Geological Institute, Russian Academy of Sciences. The REEs in Triassic sandstones in Chukotka and Wrangel Island were determined by the same method in the Laboratory of Nuclear Physics and Mass Spectral Analysis methods (Analytical Certification Test Center, Institute of Microelectronics Technology and Especially Pure Materials, Russian Academy of Sciences) under the supervision of V.K. Karandashev.

In the Th/Sc−Zr/Sc diagram (McLennan et al., 1993), samples are located in the field reflecting the recycling of sedimentary rocks, except sample 14-09, which is located in the field of provenance composition, suggesting a higher content of volcanic rock fragments therein. Based on the Zr/Sc ratio, the analyzed samples are divided into two groups (Fig. 4a): (i) group with a higher Zr/Sc value, located in the recycling field (samples 1601/1 and 1601/10 from polygon 3); (ii) group with composition variations that are very close to each other and almost similar to those in samples from Chukotka and Wrangel Island (USO-4, 14-24, 1602/14, and 14-09). It should be noted that samples 14-24 and 1602/14 include zircon populations suggesting their assignment to the Cretaceous stratigraphic interval.

Influence of the continental crust on sedimentation reflects the Th/U ratio (McLennan et al., 1993), and the Th−Th/U ratio in the diagram (Fig. 4b) allows us to trace the weathering trend in the provenance. In the Th−Th/U diagram, samples USO-4, 1601/1, 1602/14, and 14-24 are characterized by the Th/U ratio higher than 3.8, which is typical for erosion of the upper continental crust (UCC), and they are located in the field of Upper Triassic sandstones in Chukotka and Wrangel Island. The location of sample 1601/1, shifted toward a higher Th concentration, indicates a more intense weathering in the provenance or the erosion of recycled rocks. The latter assumption is likely more probable, since this sample occupies in the Th/Sc−Zr/Sc diagram a position corresponding to the maximum recycling of the detrital material among the analyzed samples. Samples 14-09 and 1601/10 are located below the 3.8 line, which most likely indicates the erosion of mainly volcanic rocks, but with different levels of weathering in the provenance (higher level in sample 1601-10 and lower level in sample 14-09).

Diagrams reflecting the provenance type based on the ratio of various elements were used to analyze the composition of eroded rocks. In the La/Th−Hf diagram (Fig 4c), the analyzed samples occupy different positions: four samples (USO-4, 1602/14, 14-24, and 14-09) are located in the field of a mixed (mafic-and-felsic rock) source; two samples (1601/1 and 1601/10) belong to the influence field of a passive continental margin. Samples USO-4 and 14-09 are located side-by-side in the field of mixed (mafic-and-felsic) rocks and almost coincide with the fields of Upper Triassic sandstones of Chukotka and Wrangel Island.

In the Co/Th−La/Sc diagram reflecting the ratio of sources of granodiorite, mafic, and felsic rocks (Gu et al., 2002), fields of the Lower Cretaceous samples from the Alpha−Mendeleev Rise coincide with those of Triassic rocks of Wrangel Island and Chukotka—they are located in the influence field of granodiorite rocks (Fig. 4d).

In the TiO$_2$−Zr diagram (Hayashi et al., 1997), the samples are divided into two groups: group 1 is represented by erosion products of intermediate rocks—data points of Triassic rocks from Chukotka and Wrangel Island (Fig. 4e); group 2, by erosion products of Cretaceous felsic rocks. Such distribution of data points of Cretaceous rocks from the Alpha−Mendeleev Rise looks somewhat strange, because these samples contain erosion products of the volcanic rocks (Skolotnev et al., 2022). Apparently, this fact is explained by the quartz−feldspar composition of the terrigenous component in sandstones formed due to the influence of river runoff (Skolotnev et al., 2022). Note that samples 14-09 and USO-4 occur in this diagram side-by-side and gravitate toward the field of Triassic rocks.

The REE distribution in all studied samples has a similar pattern on the diagrams based both on the PAAS- and chondrite-normalized values (Figs. 5a, 5b). The samples differ slightly in the REE concentration level; the curve of sample USO-4 occupies the lowest position, reflecting the lowest concentrations of these elements. The highest REE concentrations are observed in samples 1601/1 and 1601/10. Note that the location of sample 14-09 in the PAAS-normalized diagram differs from that of other samples (Fig. 5a). The spectral line of this sample rises gradually from the HREE to MREE fields and then decreases successively (but rapidly) to the LREE field, indicating the influence of mafic component represented by a high content of effusive rock fragments in sample 14-09 (Table 1).

Another important feature of REE is the Eu anomaly, which is calculated as $Eu/Eu^* = Eu_n/(Sm_nGd_n)^{1/2}$ that shows the difference between the actual Eu content and the calculated value in the REE distribution. For the UCC, the Eu/Eu* distribution is usually 0.6−0.7 (Condie, 1993; *Geochemistry ...*, 2003; McLennan et al., 1993). In all analyzed samples, the value of Eu/Eu* varies slightly from 0.62 to 0.68 (Table 2). The minimum value (0.62) is recorded in samples from Wrangel Island; the maximum (0.69), in samples from Chukotka. This ratio is 0.66 in sample USO-4. In Cretaceous samples from the Mendeleev Rise, average Eu/Eu* is 0.68.

U−Pb dating. In sample USO-4, the largest population of clastic zircons covers the range of 206−424 Ma with peaks at 206, 234, 253, 301, and 404 Ma. Older zircons are represented by single grains ranging from 548 to 2500 Ma. This age spectrum is very close that of Late Triassic sandstones in Chukotka, Wrangel Island, and western Alaska (Miller et al., 2010). Samples SS-63 and SS-65 contain a very small number of grains (14 and 20, respectively). Age peaks of zircon grains are represented by populations of 244 ± 5, 300−350, 400, 440−500, 700, and 1804 ± 20 Ma in sample SS-
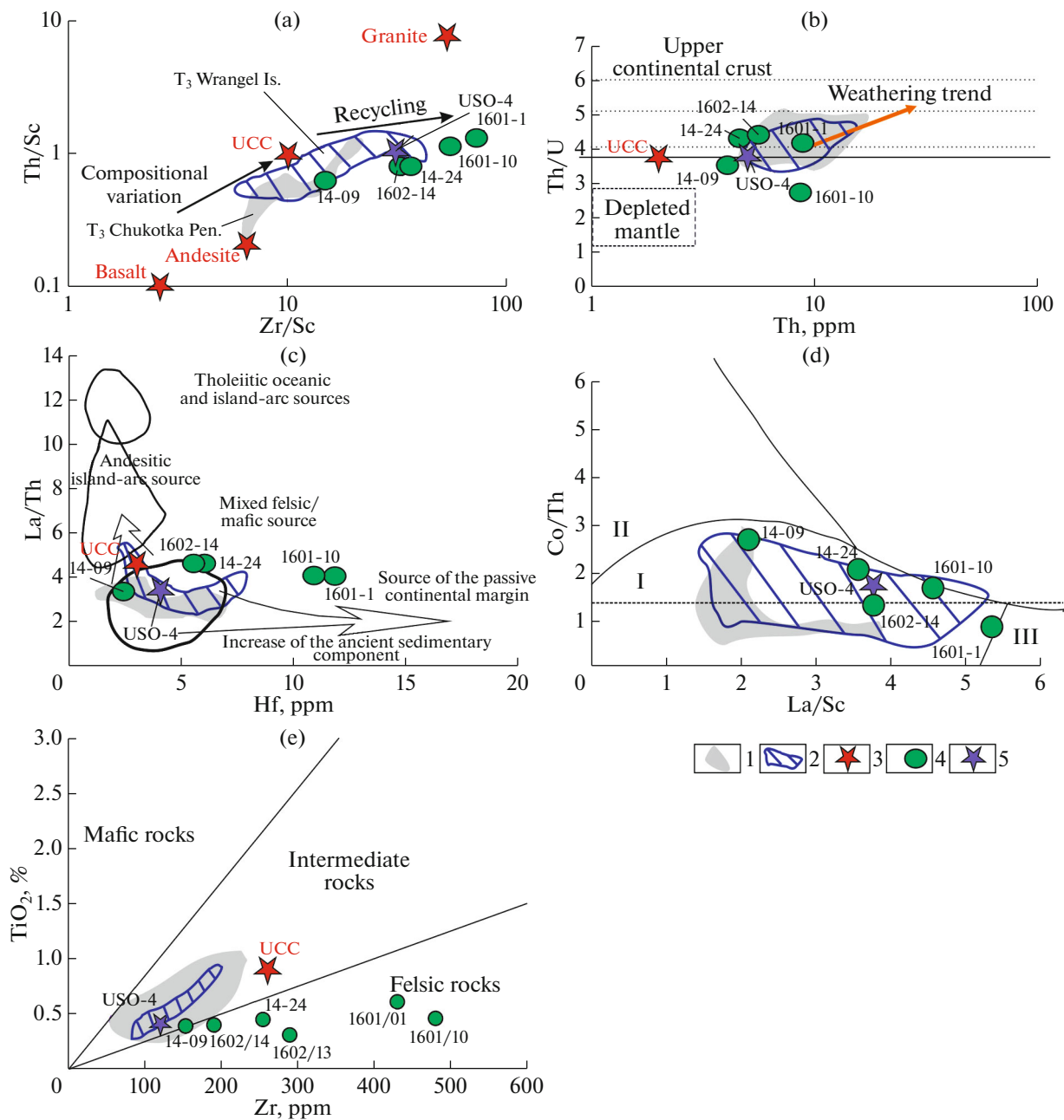
Fig. 4. Geochemical composition diagrams of the analyzed Cretaceous samples from the Mendeleev Rise in comparison with Triassic rocks in Chukotka and Wrangel Island, based on the ratios of different elements. (a) Th/Sc−Zr/Sc diagram illustrating the degree of detrital material recycling, adopted from (Taylor and McLennan, 1988, 1995); (b) Th/U−Th diagram illustrating the trend of detrital material weathering, the horizontal line with Th/U = 3.8 shows the average Th/U value in the UCC composition; (c) La/Th−Hf diagram reflecting different provenance types, classification fields are adopted from (Floyd and Leveridge, 1987); (d) Co/Th−La/Sc diagram reflecting the influence of various provenances on sedimentation, Roman numerals: (I) erosion of granodiorites or rocks with composition close to the average UCC, (II) increase in the role of mafic rocks, (III) increase in the role of felsic rocks, classification fields are adopted from (Gu et al., 2002); (e) TiO$_2$−Zr diagram (Hayashi et al., 1997), the TiO$_2$ content is adopted from (Skolotnev et al., 2022) (Table 1). (1) Composition filed of Upper Triassic sandstones in Chukotka; (2) compositions field of Upper Triassic rocks in Wrangel Island; (3) average compositions: (UCC) adopted from (*Geochemistry* ..., 2003), average Proterozoic granite and granodiorite, adopted from (Condie, 1993); (4) Cretaceous rocks of the Mendeleev Rise, according to (Skolotnev et al., 2022); (5) conventionally Triassic sample USO-4 (Shamshura Seamount).

63; by populations of 220−240 ± 4, 314 ± 7, 405−415 ± 8, 550, and 1843 ± 19 Ma, in sample SS-65. Note that the ancient age is represented by one or two grains.

In Cretaceous sandstones (samples 14-24 and 1602/14), no less than 200 zircon grains were analyzed in each sample. The zircon age spectra are fundamen-
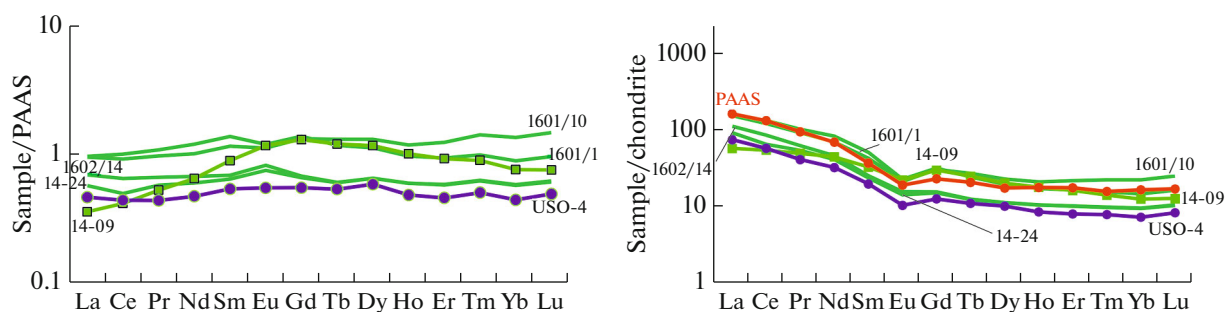
Fig. 5. Distribution of REE in the PAAS-normalized (Taylor and McLennan, 1988) and chondrite-normalized (Sun and McDonough, 1989) samples.

tally different from those of sample USO-4. In samples 14-24 and 1602/14, the youngest population of Early Cretaceous zircons includes zircons with the age range of 100−126 Ma. However, the number of such zircons is not more than 4−6 grains per sample. Grains of a wide age range (peak at 150 Ma) are scarce. The older populations include the following varieties: Hercynian cluster (peak at 270−300 Ma, sometimes complicated by a weaker peak at 250 Ma); Early Caledonian cluster (peak at 500 Ma); Paleoproterozoic cluster (peak at 1900 Ma); and Neoarchean cluster (peak at 2670 Ma). It should be noted that the diagrams of zircon populations in all Cretaceous sandstones differ markedly. Values of the ratio between populations in various samples are different—Hercynian, Proterozoic, and Archean clusters may dominate.

Nevertheless, the obvious predominance of ancient grains over Late Paleozoic−Early Mesozoic ones in samples 14-24 and 1602/14 indicates their fundamentally different structural and tectonic provenances, on the one hand, and in sample USO-4 virtually lacking this age range, on the other hand, strongly suggesting their different ages.

DISCUSSION

In the major component diagram (Fig. 3a), Cretaceous sandstones (samples 1602/14 and 1601/10) occupy boundary areas of the subarkosic field, while sample 1601/10 is characterized by a higher content of the quartz component. Sample 14-09 from polygon 2 is located at the Triassic rock boundary of Chukotka.

Table 2. Content of REE and trace elements in the studied samples

Sample no.	1601/1	1601/10	1602/14	14-24	14-09	USO-4
Sc	6.8	7.9	6.9	6.1	6.3	4.6
Cr	32	44	43	35	26	107.0
Co	7.4	14.4	7.3	24	11.0	8.6
Ni	17.2	75.1	17.6	25	26	15.7
Sr	48	63	528	365	108	116.0
Y	27	34	17.1	17.2	31	13.1
Zr	496	460	240	251	96	153.0
La	36	36	26	22	13.5	17.5
Ce	80	73	52	39	33	34.9
Pr	9.6	8.6	5.9	5.1	4.7	3.9
Nd	38	32	21	19.1	21	15.0
Sm	7.7	6.5	3.8	3.6	5.0	3.0
Eu	1.31	1.23	0.90	0.82	1.28	0.6
Gd	6.5	62	3.2	3.1	6.1	2.6
Tb	0.90	1.01	0.46	0.46	0.92	0.4
Dy	4.9	5.8	2.8	2.8	5.1	2.6
Ho	0.96	1.18	0.59	0.59	1.01	0.5
Er	2.7	3.6	1.69	1.66	2.7	1.3
Tm	0.39	0.56	0.25	0.25	0.36	0.2
Yb	2.5	3.8	1.62	1.60	2.1	1.2
Lu	0.41	0.63	0.27	0.26	0.32	0.2
Hf	11.6	10.8	5.5	5.8	2.4	4.1
Th	8.9	8.7	5.6	4.6	4.1	5.0
U	2.2	3.2	1.28	1.08	1.17	1.3

Like sample 14-09, sandstones of the Shamshura Seamount (samples SS-65 and USO-4) are located at the edge of the chosen (Chukotka−Wrangel Island) field of Triassic samples, but they are closest to the field of Triassic sandstones from Wrangel Island. In the subsidiary diagram of rock fragments, with the vertices corresponding to the contents of volcanic, metamorphic, and granitoid rocks, samples SS-85 and USO-4 are located at the boundary of Triassic sample fields (Fig. 3b), whereas Cretaceous samples make up a cluster separated from the field of Triassic rocks (Fig. 3b) and are characterized by a high content of volcanic clasts. It should be noted that quartz grains with microfractures are almost absent in samples of Cretaceous sandstones, whereas such grains are abundant and account for about one-third of the total number in sandstones from the Shamshura Seamount (Tuchkova et al., 2020).

According to the geochemical data, the Cretaceous samples, like samples from the Shamshura Seamount (samples SS-65 and USO-4), differ insignificantly and occur inside or close to the fields of Triassic rocks of Chukotka and Wrangel Island (Figs. 4a−4d). At the same time, samples 1601/10 and 1601/1 from polygon 3 are characterized by increased values of both Zr/Sc ratio and Hf content (Fig. 4c), indicating a high content of recycled rocks in the provenance for samples from the eastern polygon 3. The weathering intensity in the eroded provenance varied from moderate to low, indicating differentiated settings of the provenance. For sample USO-4, we assume that the provenance was composed of the intermediate and felsic rocks (similar in composition to the UCC) with a low content of mafic rocks. All Cretaceous samples are characterized by a significantly higher content of volcanogenic material, which is confirmed by the petrographic data.

Very shallow environments are assumed for Cretaceous samples from the Alpha−Mendeleev Rise (Skolotnev et al., 2022). This is confirmed by the microstructure of bioturbation noted in the limestone sample 1602/13, bedding in samples 14-09 and 14-24, and the presence of brecciated structure (sample 1602/14) (Skolotnev et al., 2022). The Triassic(?) rocks from the Shamshura Seamount (samples USO-4, SS-63, and SS-65) could also be deposited in a shallow-water environment (Tuchkova et al., 2020).

Based on the quartz−feldspar−rock fragments diagram (Fig. 3a), samples USO-4 and SS-65 show some similarity the Cretaceous rocks (samples 1602/14 and 14-09), but they are significant different in terms of the content of volcanic clasts (Fig. 3b). However, differences in the major component composition are not reflected fundamentally in geochemical indicators. The Eu/Eu* values differ slightly in Cretaceous and Triassic samples. In most geochemical diagrams, sample USO-4 makes up a single group with Cretaceous sandstones 14-24 and 1602/14. The REE spectra of all analyzed samples represent a single group, except sample 14-09 distinguished by the REE distribution reflecting an increased content of the mafic component. The fields of data points of Cretaceous sandstones from the Alpha−Mendeleev Rise on different geochemical diagrams coincide with those of Triassic sandstones from Wrangel Island and Chukotka (Figs. 4a−4d). The TiO$_2$−Zr ratio diagram (Fig. 4e) is an exception. Here, they form a cluster separated from the Triassic rocks and sample USO-4. All facts mentioned above can indicate a partial erosion of Triassic rocks during the deposition of Cretaceous sandstones. However, such statement needs additional research.

Samples USO-4, SS-63, and SS-65 differ in age from Cretaceous sandstones—this statement is supported strongly by sharp differences in the age spectrum pattern of detrital zircon grains extracted from these samples, indicating fundamentally different types of provenances. Similarity of the age spectra of zircons from samples USO-4, SS-63, and SS-65 to those from the Triassic sandstones of Chukotka, Wrangel Island, and western Alaska allows suggests the Late Triassic age of samples USO-4, SS-63, and SS-65.

Late Triassic sandstones are present on the Shamshura Seamount and absent at three other sites sampled in 2014 and 2016 (Skolotnev et al., 2017, 2019, 2022). Moreover, Cretaceous sandstones lie on Middle Paleozoic rocks in the sampled slope section in the southwestern part of the Mendeleev Rise. Therefore, no room is left for Triassic rocks here. Hence, either Triassic sandstones are only distributed in the Shamshura Seamount area or they were sampled insufficiently and rocks of this age range were not sampled.

CONCLUSIONS

The analyzed Triassic and Cretaceous sandy rocks from the Alpha−Mendeleev Rise are quite close to each other in terms of geochemical characteristics. However, Triassic and Cretaceous sandstones differ in petrographic features and make up two different fields in the composition diagram of the rock fragments. They are also distinguished by the specific feature of quartz grains: microfractures are almost completely absent in the Aptian sandstones, whereas they can exceed 30% in sandstones from the Shamshura Seamount. Such difference in the provenance composition was unraveled based on the U−Pb isotopic dating of detrital zircons extracted from sandstones. The Cretaceous is characterized by the predominance of ancient populations over the Late Paleozoic−Early Mesozoic varieties and the presence of a population with the age range of 100−126 Ma. The above-listed populations are absent in Triassic sandstones.

Hence, we can draw the following conclusions: the Triassic age of Shamshura Seamount sandstones in the polar part of the Mendeleev Rise is proven; sedimentological characteristics of Cretaceous and Trias-

sic sandstones of the Alpha−Mendeleev Rise are significantly different; and Triassic rocks are not widespread in this part of the Arctic.

CONFLICT OF INTEREST

The authors of this work declare that they have no conflicts of interest.

REFERENCES

Condie K.C. Chemical composition and evolution of the upper continental crust: contrasting results from surface samples and shales, *Chem. Geol.*, 1993, vol. 104, pp. 1−37.

Floyd, P.A. and Leveridge, B.E., Tectonic environment of the Devonian mode and geochemical evidence from turbiditic sandstones, *J. Geol. Soc. London*, 1987, vol. 144, pp. 531−542.

Geochemistry of Sediments and Sedimentary Rocks: Evolutionary Considerations to Mineral Deposit-Forming Environments, Geotext 4, Lenz, D.R., Ed., 2003, 184 p.

Gu, X.X., Liu, J.M., Zheng, M.H., Tang, J.X., and Qi, L., Provenance and tectonic setting of the Proterozoic turbidites in Hunan South China: geochemical evidence, *J. Sediment. Res.*, 2002, vol. 72, pp. 393−407.

Hayashi, K., Fujisawa, H., Holland, H.D., and Ohmoto, H., Geochemistry of 1.9 Ga sedimentary Rocks from northeastern Labrador, Canada, *Geochim. Cosmochim. Acta.* 1997, vol. 61, pp. 4115−4137.
https://doi.org/10.1016/S0016-7037(97)00214-7

Kossovaya, O.L., Tolmacheva, T.Yu., Petrov, O.V., Isakova, T.N., Ivanova, R.M., Mirolyubova, E.S., Rekant, P.V., and Gusev, E.A., Paleozoic carbonates and fossils of the Mendeleev Rise (eastern Arctic): a study of dredged seafloor material, *J. Geodyn.*, 2018, vol. 120, pp. 23−44.
https://doi.org/10.1016/j.jog.2018.05.001

McLennan, S.M., Hemming, S., McDaniel, D.K., and Hanson, G.N., Geochemical approaches to sedimentation, provenance, and tectonics, *Geol. Soc. Am. Spec. Pap.*, 1993, vol. 284, pp. 21−40.

Miller, E.L., Gehrels, G.E., Pease, V., and Sokolov, S., Stratigraphy and U−Pb detrital zircon geochronology of Wrangel Island, Russia: implications for Arctic paleogeography, *Am. Ass. Petrol. Geol. Bull.*, 2010, pp. 665−692.

Morozov, A.F., Petrov, O.V., Shokalsky, S.P., Kashubin, S.N., and Kremenetskii, A.A., Shkatov, M.Yu., Kaminskii, V.D., Gusev, E.A., Grikurov, G.E., Rekant, P.V., Shevchenko, S.S., Sergeev, S.A., and Shatov, V.V., New geological data substantiating the continental nature of the Central Arctic Rise zone, *Region. Geol. Metallog.*, 2013 no. 53, pp. 34−55.

Pettijohn, F.J., *Sedimentary Rocks*, New York, Harper and Row, 1975.

Skolotnev, S.G., Fedonkin, M.A., and Korniychuk, A.V., New Data on the geological structure of the southwestern Mendeleev Rise, Arcic Ocean, *Dokl. Earth Sci.*, 2017, vol. 476, pp. 1001−1006.

Skolotnev, S., Aleksandrova, G., Isakova, T., Tolmacheva, T., Kurilenko, A., Raevskaya, E., Rozhnov, S., Petrov, E., and Korniychuk, A., Fossils from seabed bedrocks: Implications for the nature of the acoustic basement of the Mendeleev Rise (Arctic Ocean), *Mar. Geol.*, 2019, vol. 407, pp. 148−163.

Skolotnev, S.G., Freiman, S.I., Khisamutdinova, A.I., Ermolaev, B.V., Okina, O.I., and Skolotneva, T.S., Sedimentary rocks in the basement of the Alpha−Mendeleev Rise, Arctic Ocean, *Lithol. Miner. Resour.*, 2022, no. 2, pp. 121−142.

Sun, S.-S. and McDonough W.F. Chemical and isotopic systematics of oceanic basalts: implications for mantle composition and processes, *Geol. Soc. Spec. Publ. London*, 1989, vol. 42, pp. 313−345.
https://doi.org/10.1144/GSL.SP.1989.042.01.19

Taylor, S.R. and McLennan, S.M., *Kontinental'naya kora: ee sostav i evolyutsiya*, Moscow: Mir, 1988.

Taylor, S.R. and McLennan, S.M., The geochemical evolution of continental crust, *Rev. Geoph.*, 1995, vol. 33, pp. 241−265.

Tuchkova, M.I., Shokalsky, S.P., Petrov, O.V., Sokolov, S.D., Sergeev, S.A., and Moiseev, A.V., Triassic deposits of Chukotka, Wrangel Island and Mendeleev Rise, Arctic Sea: sedimentology and geodynamic implications, *GFF*, 2020.
https://doi.org/10.1080/11035897.2020.1724668

Tuchkova, M.I., Sokolov, S.D., Moiseev, A.V., Verzhbitskii, V.E., Kostyleva, V.V., and Vatrushkina, E.V., Lithological characteristics of Upper Triassic sedimentary rocks in Chukotka and Wrangel Island: Interrelations with coeval rocks in the eastern Arctic, *Geol. Geofiz.*, 2023, no. 3, pp. 327−351.
https://doi.org/10.1080/11035897.2020.1724668

Translated by D. Sakya

Publisher's Note. Pleiades Publishing remains neutral with regard to jurisdictional claims in published maps and institutional affiliations.